INTERNATIONAL JOURNAL FOR NUMERICAL METHODS IN ENGINEERING
Int. J. Numer. Meth. Engng 2014; **99**:313–332
Published online 30 April 2014 in Wiley Online Library (wileyonlinelibrary.com). DOI: 10.1002/nme.4677

Error estimation and adaptivity for incompressible hyperelasticity

J. P. Whiteley[1,*,†] and S. J. Tavener[2]

[1]*Department of Computer Science, University of Oxford, Wolfson Building, Parks Road, Oxford OX1 3QD, UK*
[2]*Department of Mathematics, Colorado State University, 105 Weber Building, Fort Collins, CO 80523, USA*

SUMMARY

A Galerkin FEM is developed for nonlinear, incompressible (hyper) elasticity that takes account of nonlinearities in both the strain tensor and the relationship between the strain tensor and the stress tensor. By using suitably defined linearised dual problems with appropriate boundary conditions, *a posteriori* error estimates are then derived for both linear functionals of the solution and linear functionals of the stress on a boundary, where Dirichlet boundary conditions are applied. A second, higher order method for calculating a linear functional of the stress on a Dirichlet boundary is also presented together with an *a posteriori* error estimator for this approach. An implementation for a 2D model problem with known solution, where the entries of the strain tensor exhibit large, rapid variations, demonstrates the accuracy and sharpness of the error estimators. Finally, using a selection of model problems, the *a posteriori* error estimate is shown to provide a basis for effective mesh adaptivity. Copyright © 2014 John Wiley & Sons, Ltd.

Received 22 March 2013; Revised 17 March 2014; Accepted 26 March 2014

KEY WORDS: nonlinear elasticity; finite element; error estimation

1. INTRODUCTION

Incompressible, nonlinear elasticity has been used as a mathematical model to describe deformations of many materials including rubber [1] and biological soft tissues such as the heart [2], breast [3], skin [4], liver [5] and general soft tissue [6]. There has been a significant effort devoted to establishing conditions for the existence and uniqueness of the governing equations for this model (see, for example, [7–9] and the references therein).

The FEM is the most common numerical technique for solving the system of PDEs that describe nonlinearly elastic, incompressible deformations in response to prescribed forces, partly due to this method's ability to systematically handle irregular geometries, Neumann (traction) boundary conditions and nonlinearities. A further advantage of the FEM for incompressible, or nearly incompressible, elasticity is the available theory that may be used to guide the choice of appropriate finite element spaces. Use of appropriate spaces avoids the phenomenon known as *locking* [10–13], where the accuracy of the computed deformation is degraded by the inability of the numerical method to simultaneously satisfy both the equation governing conservation of momentum and the incompressibility constraint. The concept of locking is closely related to the discrete inf–sup condition that should be satisfied by any FEM that is used to solve Stokes equations from fluid mechanics [14], as the Stokes equations are identical to the equations of incompressible, linear elasticity [15]. For the Stokes equations—and therefore incompressible, linear elasticity—a quadratic approximation to the spatial coordinates of the deformed body and a linear approximation to a Lagrange multiplier that is introduced to enforce incompressibility, with both approximations being continuous across element boundaries, has been shown to permit computations that are free of

*Correspondence to: Jonathan P. Whiteley, Department of Computer Science, University of Oxford, Wolfson Building, Parks Road, Oxford OX1 3QD, UK.
†E-mail: jonathan.whiteley@cs.ox.ac.uk

locking [14]. Through practical computations rather than theoretical analysis, this approach has also been found to be appropriate for incompressible, nonlinear elasticity [3, 15–19]. However, to the best of our knowledge, there is no theory to guide the choice of degree of polynomial approximation for incompressible, nonlinear elasticity.

One feature of the FEM that is particularly attractive is *a posteriori* error analysis of the finite element solution (see, for example, [20–25]). This error analysis uses the computed solution and a higher order approximation to a linear dual problem to estimate the error in a given norm or functional of the solution. Furthermore, it also identifies areas of the computational domain where the contribution to the error is greatest, highlighting regions of this domain where mesh refinement may significantly improve accuracy, thus driving mesh adaptation strategies [12, 13, 20, 21, 26–29]. *A posteriori* error analysis has been attempted before for nonlinear elasticity in the special case where the strain tensor has been linearised [26, 27, 29, 30]. These authors all considered only the nonlinear relationship between the linearised strain tensor and the stress tensor. The linearisation of the strain tensor is valid only when the deformations are small, and making this assumption prevents the application to scenarios where large deformations, such as those commonly seen in biology, may occur. We have already noted the similarities in challenges in applying the FEM to incompressible fluid flow problems and incompressible elasticity. *A posteriori* error estimators have been derived for the (linear) incompressible Stokes equations [31]. *A posteriori* techniques have been applied to nonlinear elasticity for the case of almost incompressible elasticity [32]. However, when *a posteriori* techniques were applied to fully incompressible nonlinear elasticity [26, 27], the linearised strain tensor was used to enforce incompressibility, which will clearly be incorrect for large deformations.

A common quantity of interest from a finite element solution is an integral of the normal derivative of the solution across some specified part of the boundary where Dirichlet boundary conditions are prescribed. For example, in solid mechanics applications, we may wish to calculate the total force or moment about a point (i.e. some function of the derivatives of the solution) acting on some part of a boundary where displacements are specified (i.e. Dirichlet boundary conditions are applied). When modelling small deflections of a clamped beam [33–35] or electrochemical processes [28, 36], higher-order convergence of these functionals has been obtained by rewriting these functionals as an integral over the interior of the computational domain.

In this study, we use the full nonlinear theory of incompressible, nonlinear elasticity, without the restrictions made by other authors of linearising the strain tensor. We derive *a posteriori* error estimates for two different classes of functionals of the solution: (i) functionals that are integrals of the solution over some region of the interior of the computational domain and (ii) functionals that are integrals of the stress acting on a part of the boundary where Dirichlet boundaries are specified. For the second class of functionals, we derive alternative *a posteriori* error estimates when the functionals are rewritten as an integral over the interior of the computational domain. This employs the mathematical 'trick', previously described, which has been previously used by other authors [28, 33–36] for different applications but does not appear to be commonly used in other application domains including those that utilise incompressible nonlinear elasticity. The performance of these error estimators is then investigated for a variety of functionals through computations relating to model problems with large deformations. Finally, the error estimators are used to drive adaptivity of the finite element mesh. Throughout this study, we have attempted to keep the derivations of the error estimators as simple as possible so that the theory is accessible to a wide audience: some technical definitions, for example, the function spaces used, are however necessary for mathematical rigour.

2. THE GOVERNING EQUATIONS

In this section, we give a brief description of the governing equations. For more details, see, for example, Howell *et al.* [1]. Let $\mathbf{X}$ denote the coordinates of an undeformed, incompressible body that occupies a bounded region of space $\Omega \subset \Re^d$, and $\mathbf{x}$ denote the coordinates of the deformed body. If $d = 2$, then the components of $\mathbf{X}$ are given by $\mathbf{X} = (X_1, X_2)^\top$, if $d = 3$ then $\mathbf{X} = (X_1, X_2, X_3)^\top$. The components of $\mathbf{x}$, and other vectors used in this study, follow a similar pattern. The deformation gradient tensor F has entries given by

DOI: 10.1002/nme

$$F_{iM} = \frac{\partial x_i}{\partial X_M}, \qquad i, M = 1, \ldots, d.$$

If $S = S(F)$ represents the first Piola–Kirchhoff stress tensor, $\mathbf{g}$ represents the body force per unit mass and ρ is the (constant) density of the incompressible body then static, elastic deformations result in coordinates of the deformed body $\mathbf{x}$ that satisfy

$$\frac{\partial S_{Mi}}{\partial X_M} + \rho g_i = 0, \qquad i = 1, \ldots, d, \tag{1}$$

$$\det F = 1, \tag{2}$$

for $\mathbf{X} \in \Omega$, where in the previous text and throughout we use the summation convention. We partition the boundary $\partial\Omega$ into a Dirichlet boundary $\partial\Omega_D$, where displacement boundary conditions are specified, and a Neumann boundary $\partial\Omega_N$, where traction boundary conditions are specified. Suitable boundary conditions are

$$x_i = x_i^0, \qquad i = 1, \ldots, d, \qquad \mathbf{X} \in \partial\Omega_D, \tag{3}$$

$$S_{Mi} N_M = s_i^0, \qquad i = 1, \ldots, d, \qquad \mathbf{X} \in \partial\Omega_N, \tag{4}$$

where x_i^0, s_i^0, $i = 1, \ldots, d$, are specified functions and $\mathbf{N}$ is the outward pointing unit normal to the undeformed body. In common with Ortner and Süli [37], we assume that $\mathbf{g} \in L_2(\Omega)^d$ and $s_i^0 \in L_2(\partial\Omega_N)$.

If the body is hyperelastic, then Equations (1)–(4) are closed by specifying a constitutive relation that specifies entries of S in terms of both F and the Lagrange multiplier p that is used to enforce the incompressibility condition given by Equation (2). In particular,

$$S_{Mi} = \frac{\partial W}{\partial F_{iM}} - p \det(F) F^{-1}_{Mi}, \qquad M, i = 1, \ldots, d, \tag{5}$$

where $W = W(F)$ is known as the *strain energy density* and $W \in C^4(\Re^{d\times d}, \Re)$, [37]. Note the presence of the term $\det(F)$ in Equation (5) even though this term is identically equal to 1. The purpose of this will become clear when we write the weak form of Equations (1) and (2) in saddle point form in Section 3.2.

We noted in Section 1 that some other authors who had investigated nonlinear elasticity used a linearisation of the strain tensor, and so, their results were only valid for small deformations [26, 27, 29, 30]. Our approach of using the first Piola–Kirchhoff stress tensor S implies that we are using both a nonlinear relationship between strain and displacement as well as the nonlinear Green–Lagrange strain tensor E, as we shall now demonstrate. The Green–Lagrange strain tensor satisfies $E = \frac{1}{2}\left(F^\top F - \mathcal{I}\right)$, where $\mathcal{I}$ is the identity tensor. Entries of the second Piola–Kirchoff stress tensor T are given by

$$T_{MN} = \frac{\partial W}{\partial E_{MN}} - p \det(F) F^{-1}_{Mi} F^{-1}_{Ni}, \qquad M, N = 1, \ldots, d.$$

Clearly, T takes account of both linearities in the stress–strain relationship (through the functional form of W) and the nonlinear strain tensor E. Using the relationship $S = TF^\top$ between stress tensors, we see that S must also take account of both nonlinearities.

3. THE FINITE ELEMENT SOLUTION

3.1. Mathematical preliminaries

We assume that the domain on which the solution is defined, Ω, has been partitioned into a conforming mesh of elements κ with no hanging nodes. We define $L_2(\Omega)$ to be the space of square integrable functions defined on Ω:

DOI: 10.1002/nme

$$L_2(\Omega) = \left\{ v : \int_\Omega v^2 \, \mathrm{d}V < \infty \right\},$$

and the Sobolev space, $H^1(\Omega)$, and various subsets of the Sobolev space that we will require by

$$\begin{aligned}
H^1(\Omega) &= \left\{ v \in L_2(\Omega) : \frac{\partial v}{\partial X_M} \in L_2(\Omega), M = 1, \ldots, d \right\}, \\
H^1_E(\Omega) &= \left\{ v \in H^1(\Omega) : v \text{ satisfies prescribed Dirichlet boundary conditions} \right\}, \\
H^1_{E_0}(\Omega) &= \left\{ v \in H^1(\Omega) : v = 0 \text{ for } \mathbf{X} \in \partial\Omega_D \right\}, \\
H^1_y(\Omega) &= \left\{ v \in H^1(\Omega) : v = y \text{ for } \mathbf{X} \in \partial\Omega_D, \text{where } y(\mathbf{X}) \text{ is a specified function} \right\}.
\end{aligned}$$

We now discuss the function spaces used for the finite element solution. Throughout this study, we use a finite element mesh with no hanging nodes. When deriving the finite element approximation to the solution, we will use triangular elements in two dimensions, or tetrahedral elements in three dimensions, but we note that an almost identical analysis could be carried out for quadrilateral (if $d = 2$) or hexahedral (if $d = 3$) elements. We define $P^k(\Omega)$ to be the set of continuous functions that are polynomials of degree k when restricted to a given element. Subsets $P^k_E(\Omega)$ and $P^k_{E_0}(\Omega)$ of $P^k(\Omega)$ are defined in an analogous manner to the subsets $H^1_E(\Omega)$ and $H^1_{E_0}(\Omega)$ of the Sobolev space $H^1(\Omega)$.

The definitions of the aforementioned function spaces may be extended to vector valued functions, for example,

$$\left[H^1(\Omega)\right]^2 = H^1(\Omega) \times H^1(\Omega).$$

3.2. *The weak solution*

We write the weak solution in saddle point form and highlight the role of the incompressibility constraint. Firstly, we define

$$S^c_{Mi} = \frac{\partial W}{\partial F_{iM}}, \qquad i, M = 1, \ldots, d,$$

where the superscript c is used to denote the contribution to S that is not used to enforce incompressibility. The weak form of Equations (1) and (2) is the following: find $\mathbf{x} \in \left[H^1_E(\Omega)\right]^d$, $p \in L_2(\Omega)$ such that, for all $\mathbf{v} \in \left[H^1_{E_0}(\Omega)\right]^d$, $q \in L_2(\Omega)$,

$$a(\mathbf{x}, \mathbf{v}) - b(\mathbf{x}, p, \mathbf{v}) = l_1(\mathbf{v}), \tag{6}$$

$$b(\mathbf{x}, q, \mathbf{x}) = l_2(q), \tag{7}$$

where

$$\begin{aligned}
a(\mathbf{x}, \mathbf{v}) &= \int_\Omega S^c_{Mi} \frac{\partial v_i}{\partial X_M} \, \mathrm{d}V, \\
b(\mathbf{x}, p, \mathbf{v}) &= \int_\Omega p \det(F) F^{-1}_{Mi} \frac{\partial v_i}{\partial X_M} \, \mathrm{d}V, \\
l_1(\mathbf{v}) &= \int_\Omega \rho g_i v_i \, \mathrm{d}V + \int_{\partial\Omega_N} s^0_i v_i \, \mathrm{d}S, \\
l_2(q) &= \int_\Omega dq \, \mathrm{d}V.
\end{aligned}$$

We do not consider the existence and uniqueness of the solution to Equations (6) and (7) or the function spaces in which any solutions lie. We have used Sobolev spaces only to guarantee that the integrals required for the remainder of this study are well defined and assume that a solution exists.

DOI: 10.1002/nme

Defining $\hat{\mathbf{x}}$, $\hat{\mathbf{v}}$ by

$$\hat{\mathbf{x}} = \begin{pmatrix} \mathbf{x} \\ p \end{pmatrix}, \qquad \hat{\mathbf{v}} = \begin{pmatrix} \mathbf{v} \\ q \end{pmatrix},$$

we write Equations (6) and (7) in the more compact form: find $\hat{\mathbf{x}} \in \left[H^1_E(\Omega)\right]^d \times L_2(\Omega)$, such that, for all $\hat{\mathbf{v}} \in \left[H^1_{E_0}(\Omega)\right]^d \times L_2(\Omega)$

$$A(\hat{\mathbf{x}}, \hat{\mathbf{v}}) = L(\hat{\mathbf{v}}), \tag{8}$$

where

$$\begin{aligned} A(\hat{\mathbf{x}}, \hat{\mathbf{v}}) &= \int_\Omega S_{Mi} \frac{\partial v_i}{\partial X_M} + q \det F \, \mathrm{d}V, \\ L(\hat{\mathbf{v}}) &= \int_\Omega \rho g_i v_i + q \, \mathrm{d}V + \int_{\partial\Omega_N} s_i^0 v_i \, \mathrm{d}S. \end{aligned}$$

The factor of d that is seen in the expression for $l_2(q)$ in the previous text disappears from Equation (8) on noting that, when evaluating Equation (7), we have

$$F^{-1}_{Mi} \frac{\partial x_i}{\partial X_M} = F^{-1}_{Mi} F_{iM} = d,$$

and so,

$$\begin{aligned} b(\mathbf{x}, q, \mathbf{x}) &= \int_\Omega q \det(F) F^{-1}_{Mi} \frac{\partial x_i}{\partial X_M} \, \mathrm{d}V \\ &= \int_\Omega q \det(F) F^{-1}_{Mi} F_{iM} \, \mathrm{d}V \\ &= \int_\Omega dq \, \mathrm{d}V. \end{aligned}$$

We may cancel the factor of d on both sides of Equation (7).

3.3. *The finite element solution*

Define $\hat{\mathbf{x}}^h$, $\hat{\mathbf{v}}^h$ by

$$\hat{\mathbf{x}}^h = \begin{pmatrix} \mathbf{x}^h \\ p^h \end{pmatrix}, \qquad \hat{\mathbf{v}}^h = \begin{pmatrix} \mathbf{v}^h \\ q^h \end{pmatrix}.$$

The finite element solution that we will use in this study is the following: find $\hat{\mathbf{x}}^h \in \left[P^k_E(\Omega)\right]^d \times P^{k-1}(\Omega)$, such that, for all $\hat{\mathbf{v}}^h \in \left[P^k_{E_0}(\Omega)\right]^d \times P^{k-1}(\Omega)$, with $k = 2, 3, 4, \ldots$,

$$A\left(\hat{\mathbf{x}}^h, \hat{\mathbf{v}}^h\right) = L\left(\hat{\mathbf{v}}^h\right). \tag{9}$$

4. *A POSTERIORI* ERROR ANALYSIS

Our *a posteriori* error analysis is similar in spirit to that presented for other PDEs by Becker and Rannacher [24] and Giles and Süli [21]. We first consider functionals defined over the whole domain Ω in Section 4.1 before considering functionals defined over $\partial\Omega_D$ in Section 4.2. In both cases, we first linearise $A(\cdot,\cdot)$ before interchanging the role of the first and second arguments of $A(\cdot,\cdot)$ when defining the dual problem. We then demonstrate how this mathematical machinery allows us to write the error in the linear functional estimated using the finite element solution as an expression

DOI: 10.1002/nme

involving only the dual solution, the residual when the finite element solution is substituted into the PDE and, if desired, a projection of the dual solution into the finite element space.

4.1. Error estimator for functionals defined over Ω

Suppose we wish to compute a linear functional $J_\Omega(\hat{\mathbf{x}})$ of the solution of Equations (1)–(5), where the functional is the integral of some inner product over the region Ω. Under these circumstances,

$$J_\Omega(\hat{\mathbf{x}}) = \int_\Omega \hat{\mathbf{y}}(\mathbf{X}) \cdot \hat{\mathbf{x}} \, \mathrm{d}V, \tag{10}$$

where $\hat{\mathbf{y}}(\mathbf{X})$ is a specified function.

4.1.1. The dual problem. We first present a linearisation of $A(\cdot,\cdot)$ that will allow us to define a suitable linear adjoint problem. The solution of this adjoint problem will be used when deriving our error estimate. Defining

$$C_{ijMN}(F,p) = \frac{\partial S_{Mi}}{\partial F_{jN}}, \qquad i,j,M,N = 1,\ldots,d,$$
$$D_{iM}(F,p) = \frac{\partial S_{Mi}}{\partial p}, \qquad i,M = 1,\ldots,d,$$

we will require the quantities

$$\bar{C}_{ijMN} = \int_0^1 C_{ijMN}(\alpha(s),\beta(s)) \, \mathrm{d}s, \qquad i,j,M,N = 1,\ldots,d, \tag{11}$$

$$\bar{D}_{iM} = \int_0^1 D_{iM}(\alpha(s),\beta(s)) \, \mathrm{d}s, \qquad i,M = 1,\ldots,d, \tag{12}$$

where

$$\alpha(s) = sF + (1-s)F^h,$$
$$\beta(s) = sp + (1-s)p^h,$$

and F^h is the deformation gradient tensor calculated using $\mathbf{x} = \mathbf{x}^h$. We may then write, for $i, M = 1,\ldots,d$,

$$\begin{aligned}\bar{C}_{ijMN}(F_{jN} - F^h_{jN}) + \bar{D}_{iM}(p - p^h) &= \int_0^1 C_{ijMN}(\alpha,\beta)\frac{\partial \alpha_{jN}}{\partial s} + D_{iM}\frac{\partial \beta}{\partial s} \, \mathrm{d}s \\ &= \int_0^1 \frac{\partial S_{Mi}}{\partial F_{jN}}\frac{\partial \alpha_{jN}}{\partial s} + \frac{\partial S_{Mi}}{\partial p}\frac{\partial \beta}{\partial s} \, \mathrm{d}s \\ &= \int_0^1 \frac{\partial S_{Mi}}{\partial s} \, \mathrm{d}s \\ &= S_{Mi} - S^h_{Mi},\end{aligned} \tag{13}$$

where S^h_{Mi} is the first Piola–Kirchhoff stress tensor evaluated at $\hat{\mathbf{x}} = \hat{\mathbf{x}}^h$.

Using Equation (5) and noting that

$$\frac{\partial}{\partial F_{iM}}(\det(F)) = F^{-1}_{Mi}\det(F), \qquad i,M = 1,\ldots,d,$$

we may deduce that

$$D_{iM} = -\frac{\partial}{\partial F_{iM}}(\det(F)). \qquad i,M = 1,\ldots,d, \tag{14}$$

DOI: 10.1002/nme

Hence,

$$\begin{aligned}\bar{D}_{iM}(F_{iM} - F^h_{iM}) &= \int_0^1 D_{iM}(\alpha)\frac{\partial \alpha_{iM}}{\partial s}\,\mathrm{d}s \\ &= \int_0^1 -\frac{\partial}{\partial F_{iM}}(\det(F))\frac{\partial \alpha_{iM}}{\partial s}\,\mathrm{d}s \\ &= \int_0^1 -\frac{\partial}{\partial s}\left(\det(F)\right)\,\mathrm{d}s \\ &= -\det(F) + \det\left(F^h\right).\end{aligned} \tag{15}$$

We are now in a position to define the bilinear operator $\bar{A}(\cdot,\cdot)$ that will be used to specify our dual problem. Let

$$\hat{\mathbf{w}} = \begin{pmatrix}\mathbf{w}\\ r\end{pmatrix}, \qquad \hat{\phi} = \begin{pmatrix}\boldsymbol{\phi}\\ \psi\end{pmatrix},$$

we define $\bar{A}(\mathbf{w},\hat{\phi})$ to be

$$\bar{A}\left(\mathbf{w},\hat{\phi}\right) = \int_\Omega \left(\bar{C}_{ijMN}\frac{\partial w_j}{\partial X_N} + \bar{D}_{iM}r\right)\frac{\partial \phi_i}{\partial X_M} - \bar{D}_{iM}\frac{\partial w_i}{\partial X_M}\psi\,\mathrm{d}V. \tag{16}$$

It follows from the definition of $\bar{A}(\cdot,\cdot)$, and from Equations (13)–(15), that

$$\bar{A}\left(\hat{\mathbf{x}} - \hat{\mathbf{x}}^h, \hat{\phi}\right) = A\left(\hat{\mathbf{x}},\hat{\phi}\right) - A\left(\hat{\mathbf{x}}^h,\hat{\phi}\right). \tag{17}$$

The appropriate dual problem in this case is the following: find $\hat{\phi} \in \left[H^1_{E_0}(\Omega)\right]^d \times L_2(\Omega)$ such that, for all $\hat{\mathbf{w}} \in \left[H^1_{E_0}(\Omega)\right]^d \times L_2(\Omega)$

$$\bar{A}\left(\hat{\mathbf{w}},\hat{\phi}\right) = J_\Omega\left(\hat{\mathbf{w}}\right). \tag{18}$$

Note that the roles of the first and second aforementioned arguments, the reverse of those in Equation (8), indicate that this is the adjoint operator. The PDE satisfied by $\hat{\phi}$ is given in Section 4.1.2. In practice, as the true solution $\hat{\mathbf{x}}$ is unknown, the quantities $\bar{C}, \bar{D}$ are evaluated at $\hat{\mathbf{x}} = \hat{\mathbf{x}}^h$. The accuracy of this approximation improves as the finite element solution is refined.

We may now write:

$$\begin{aligned}J_\Omega\left(\hat{\mathbf{x}}\right) - J_\Omega\left(\hat{\mathbf{x}}^h\right) &= J_\Omega\left(\hat{\mathbf{x}} - \hat{\mathbf{x}}^h\right) && \text{by linearity of } J_\Omega(\cdot) \\ &= \bar{A}\left(\hat{\mathbf{x}} - \hat{\mathbf{x}}^h, \hat{\phi}\right) && \text{by Equation (18), assuming } \hat{\mathbf{x}} - \hat{\mathbf{x}}^h = \mathbf{0} \text{ for } \mathbf{X} \in \partial\Omega_D, \\ &= A\left(\hat{\mathbf{x}},\hat{\phi}\right) - A\left(\hat{\mathbf{x}}^h,\hat{\phi}\right) && \text{by Equation (17)} \qquad (19) \\ &= L\left(\hat{\phi}\right) - A\left(\hat{\mathbf{x}}^h,\hat{\phi}\right) && \text{by Equation (8), as } \hat{\phi} \in H^1_{E_0}, \\ &= \int_{\partial\Omega_N} s^0_i\phi_i\,\mathrm{d}S + \int_\Omega \rho g_i\phi_i - S^h_{Mi}\frac{\partial \phi_i}{\partial X_M} + \psi\left(1 - \det(F^h)\right)\,\mathrm{d}V && (20) \\ &= \int_{\partial\Omega_N} s^0_i\phi_i\,\mathrm{d}S + \int_\Omega \phi_i\left(\rho g_i + \frac{\partial S^h_{Mi}}{\partial X_M}\right) + \psi\left(1 - \det(F^h)\right)\,\mathrm{d}V \\ &\quad - \sum_\kappa \int_{\partial\kappa} S^h_{Mi}\phi_i N_M\,\mathrm{d}S. && (21)\end{aligned}$$

DOI: 10.1002/nme

Noting that Equations (8) and (9) yield, for all $\hat{\mathbf{v}}^h \in \left[P^k_{E_0}(\Omega)\right]^d \times P^{k-1}(\Omega)$, where $k = 2, 3, 4, \ldots$, the orthogonality property

$$A\left(\hat{\mathbf{x}}, \hat{\mathbf{v}}^h\right) - A\left(\hat{\mathbf{x}}^h, \hat{\mathbf{v}}^h\right) = 0, \tag{22}$$

and that $A(\cdot,\cdot)$ is linear in the second argument, we may combine Equations (19) and (22) to give

$$J_\Omega\left(\hat{\mathbf{x}}\right) - J_\Omega\left(\hat{\mathbf{x}}^h\right) = A\left(\hat{\mathbf{x}}, \hat{\phi} - \hat{\mathbf{v}}^h\right) - A\left(\hat{\mathbf{x}}^h, \hat{\phi} - \hat{\mathbf{v}}^h\right).$$

Proceeding in the same way as previously mentioned when obtaining Equations (20) and (21), but with $\hat{\phi}$ replaced by $\hat{\phi} - \hat{\mathbf{v}}^h$, and choosing $\hat{\mathbf{v}}^h$ to be $\hat{\phi}^{\mathcal{I}}$, the interpolant of $\hat{\phi}$ into the finite element space, yields

$$\begin{aligned}
&J_\Omega\left(\hat{\mathbf{x}}\right) - J_\Omega\left(\hat{\mathbf{x}}^h\right) \\
&\quad = \int_{\partial\Omega_N} s_i^0\left(\phi_i - \phi_i^{\mathcal{I}}\right)\,\mathrm{d}S \\
&\qquad + \int_\Omega \rho g_i\left(\phi_i - \phi_i^{\mathcal{I}}\right) - S^h_{Mi}\frac{\partial}{\partial X_M}\left(\phi_i - \phi_i^{\mathcal{I}}\right) \\
&\qquad + \left(\psi - \psi^{\mathcal{I}}\right)\left(1 - \det(F^h)\right)\,\mathrm{d}V \qquad (23)\\
&\quad = \int_{\partial\Omega_N} s_i^0\left(\phi_i - \phi_i^{\mathcal{I}}\right)\,\mathrm{d}S \\
&\qquad + \int_\Omega \left(\phi_i - \phi_i^{\mathcal{I}}\right)\left(\rho g_i + \frac{\partial S^h_{Mi}}{\partial X_M}\right) + \left(\psi - \psi^{\mathcal{I}}\right)\left(1 - \det(F^h)\right)\,\mathrm{d}V \\
&\qquad - \sum_\kappa \int_{\partial\kappa} S^h_{Mi}\left(\phi_i - \phi_i^{\mathcal{I}}\right) N_M\,\mathrm{d}S. \qquad (24)
\end{aligned}$$

Equations (20), (21), (23) and (24) are four estimates of the error of the functional in terms of the finite element solution and the dual solution. It should be noted that, in general, we cannot obtain an analytic solution for the dual problem $\hat{\phi}$. In practice, $\hat{\phi}$ is estimated by computing on either a finer mesh or by using higher-order approximating polynomial functions on each element.

4.1.2. The PDE satisfied by the dual solution. For $J_\Omega(\hat{\mathbf{x}}) = \langle \hat{\mathbf{y}} \cdot \hat{\mathbf{x}} \rangle$, where $\hat{\mathbf{y}} = (\mathbf{y} \quad s)^\top$, manipulation of Equations (16) and (18) reveals that the (adjoint) PDE satisfied by $\hat{\phi}$ is

$$\begin{aligned}
-\frac{\partial}{\partial X_M}\left(\bar{C}_{ijQM}\frac{\partial \phi_i}{\partial X_Q} - \bar{D}_{jM}\psi\right) &= \mathbf{y}, \qquad j = 1, \ldots, d,\\
\bar{D}_{jM}\frac{\partial \phi_j}{\partial X_M} &= s,
\end{aligned}$$

for $\mathbf{X} \in \Omega$, subject to boundary conditions

$$\begin{aligned}
\phi_j &= 0, \qquad j = 1, 2, 3, \qquad \mathbf{X} \in \partial\Omega_D,\\
-\left(\bar{C}_{ijQM}\frac{\partial \phi_i}{\partial X_Q} - \bar{D}_{jM}\psi\right) N_M &= 0, \qquad j = 1, 2, 3, \qquad \mathbf{X} \in \partial\Omega_N.
\end{aligned}$$

In practice, $\bar{C}_{ijQM}, \bar{D}_{jM}, i, j, Q, M = 1, \ldots, d$ are evaluated by taking $\alpha = F^h$ and $\beta = p^h$ in Equations (11) and (12). This approximation is discussed in Section 4.3.

DOI: 10.1002/nme

4.2. Error estimator for functionals defined over $\partial\Omega_D$

Suppose we wish to compute some functional $J_{\partial\Omega_D}(\hat{\mathbf{x}})$ of the solution of Equations (1)–(5), where the functional is some weighted integral of the traction over part (or all) of the Dirichlet boundary. The functional can then be written as

$$J_{\partial\Omega_D}(\hat{\mathbf{x}}) = \int_{\partial\Omega_D} \hat{\mathbf{y}}(\mathbf{X}) \cdot \hat{\mathbf{t}} \, \mathrm{d}V, \tag{25}$$

where $\hat{\mathbf{t}} = (\mathbf{t}\ 0)^\top$ with $t_i = S_{Mi} N_M,\ i = 1, \ldots, d$, and $\hat{\mathbf{y}} = (\mathbf{y}\ 0)^\top$.

4.2.1. Direct evaluation of the functional. The functional given by Equation (25) may be estimated by computing the finite element solution and substituting this solution into the functional as it is written. Duality can again be used to estimate the error in the computed value of the functional. The appropriate dual problem is the following: find $\hat{\boldsymbol{\phi}} \in \left[H^1_{\mathbf{y}}(\Omega)\right]^d \times L_2(\Omega)$ such that, for all $\hat{\mathbf{w}} \in \left[H^1_{E_0}(\Omega)\right]^d \times L_2(\Omega)$

$$\bar{A}(\hat{\mathbf{w}}, \hat{\phi}) = 0. \tag{26}$$

On noting that the linearisation in Equation (17) is valid for $\hat{\boldsymbol{\phi}} \in \left[H^1_{\mathbf{y}}(\Omega)\right]^d \times L_2(\Omega)$, we may then write

$$\begin{aligned}
0 &= \bar{A}(\hat{\mathbf{x}} - \hat{\mathbf{x}}^h, \hat{\phi}) \\
&= A(\hat{\mathbf{x}}, \hat{\phi}) - A(\hat{\mathbf{x}}^h, \hat{\phi}) \qquad \text{using Equation (17)} \\
&= L(\hat{\phi}) + J_{\partial\Omega_D}(\hat{\mathbf{x}}) - A(\hat{\mathbf{x}}^h, \hat{\phi}) \qquad \text{by applying the divergence theorem} \\
&= J_{\partial\Omega_D}(\hat{\mathbf{x}}) + \int_\Omega \phi_i \left(\rho g_i + \frac{\partial S^h_{Mi}}{\partial X_M}\right) + \psi\left(1 - \det(F^h)\right) \mathrm{d}V + \int_{\partial\Omega_N} s^0_i \phi_i \, \mathrm{d}S \\
&\quad - \sum_\kappa \int_{\partial\kappa} S^h_{Mi} \phi_i N_M \, \mathrm{d}S.
\end{aligned}$$

Rearranging, we obtain

$$\begin{aligned}
J_{\partial\Omega_D}(\hat{\mathbf{x}}) - J_{\partial\Omega_D}(\hat{\mathbf{x}}^h) = &- \int_\Omega \phi_i \left(\rho g_i + \frac{\partial S^h_{Mi}}{\partial X_M}\right) + \psi\left(1 - \det(F^h)\right) \mathrm{d}V \\
&- \int_{\partial\Omega_N} s^0_i \phi_i \, \mathrm{d}S + \sum_\kappa \int_{\partial\kappa/\partial\Omega_D} S^h_{Mi} \phi_i N_M \, \mathrm{d}S.
\end{aligned} \tag{27}$$

Note the similarities between this identity and Equation (21).

4.2.2. Indirect evaluation of the functional. Let $\hat{\boldsymbol{\alpha}} = (\boldsymbol{\alpha}\ \beta)^\top$ be any continuous function in $\left[H^1(\Omega)\right]^d \times L_2(\Omega)$ such that $\boldsymbol{\alpha} = \mathbf{y}$ on $\partial\Omega_D$. An alternative method for computing the functional given by Equation (25) is to take the scalar product of Equations (1) and (2) with $\hat{\boldsymbol{\alpha}}$ and integrate over Ω to give

$$\int_\Omega \alpha_i \left(\frac{\partial S_{Mi}}{\partial X_M} + \rho g_i\right) + \beta\,(1 - \det(F))\ \mathrm{d}V = 0.$$

Applying the divergence theorem to the first term yields

$$J_{\partial\Omega_D}(\hat{\mathbf{x}}) = A(\hat{\mathbf{x}}, \hat{\boldsymbol{\alpha}}) - L(\hat{\boldsymbol{\alpha}}). \tag{28}$$

DOI: 10.1002/nme

Provided $\boldsymbol{\alpha} = \mathbf{y}$ for $\mathbf{X} \in \partial\Omega_D$, evaluation of $J_{\partial\Omega_D}(\hat{\mathbf{x}})$ is independent of the choice of $\hat{\boldsymbol{\alpha}}$. Suppose $\boldsymbol{\alpha_1}, \boldsymbol{\alpha_2} = \mathbf{y}$ for $\mathbf{X} \in \partial\Omega_D$, and let J_1, J_2 be the values of the functional calculated from these two functions. We then have

$$\begin{aligned} J_1 - J_2 &= A(\hat{\mathbf{x}}, \hat{\boldsymbol{\alpha}}_1) - L(\hat{\boldsymbol{\alpha}}_1) - A(\hat{\mathbf{x}}, \hat{\boldsymbol{\alpha}}_2) + L(\hat{\boldsymbol{\alpha}}_2) \\ &= A(\hat{\mathbf{x}}, \hat{\boldsymbol{\alpha}}_1 - \hat{\boldsymbol{\alpha}}_2) - L(\hat{\boldsymbol{\alpha}}_1 - \hat{\boldsymbol{\alpha}}_2) \qquad \text{by linearity of second argument of } A(\cdot,\cdot) \\ &= L(\hat{\boldsymbol{\alpha}}_1 - \hat{\boldsymbol{\alpha}}_2) - L(\hat{\boldsymbol{\alpha}}_1 - \hat{\boldsymbol{\alpha}}_2) \qquad \text{using Equation (9)} \\ &= 0, \end{aligned}$$

and so the value of $J_{\partial\Omega_D}$ is independent of the choice of $\hat{\boldsymbol{\alpha}}$.

We now derive an error estimator for the functional calculated by Equation (28). Let $\hat{\boldsymbol{\phi}}$ be the solution of the dual problem given by Equation (26) and $\hat{\phi}^{\mathcal{I}}$ be the interpolation of $\hat{\boldsymbol{\phi}}$ onto the finite element space. Clearly, $\hat{\phi}^{\mathcal{I}} \in \left[H^1_{\mathbf{y}}(\Omega)\right]^d \times L_2(\Omega)$, and

$$J_{\partial\Omega_D}(\hat{\mathbf{x}}) \quad = \quad A\left(\hat{\mathbf{x}}, \hat{\phi}^{\mathcal{I}}\right) - L\left(\hat{\phi}^{\mathcal{I}}\right).$$

We may then estimate $J_{\partial\Omega_D}$ from the finite element solution using

$$J_{\partial\Omega_D}\left(\hat{\mathbf{x}}^h\right) \quad = \quad A\left(\hat{\mathbf{x}}^h, \hat{\phi}^{\mathcal{I}}\right) - L\left(\hat{\phi}^{\mathcal{I}}\right).$$

We may now write

$$\begin{aligned} J_{\partial\Omega_D}(\hat{\mathbf{x}}) - J_{\partial\Omega_D}\left(\hat{\mathbf{x}}^h\right) &= A\left(\hat{\mathbf{x}}, \hat{\phi}^{\mathcal{I}}\right) - A\left(\hat{\mathbf{x}}^h, \hat{\phi}^{\mathcal{I}}\right) \\ &= A\left(\hat{\mathbf{x}}, \hat{\phi}^{\mathcal{I}}\right) - A\left(\hat{\mathbf{x}}^h, \hat{\phi}^{\mathcal{I}}\right) - \bar{A}(\hat{\mathbf{x}} - \hat{\mathbf{x}}^h, \hat{\phi}) \qquad \text{by Equation (26)} \\ &= A\left(\hat{\mathbf{x}}, \hat{\phi}^{\mathcal{I}}\right) - A\left(\hat{\mathbf{x}}^h, \hat{\phi}^{\mathcal{I}}\right) - A(\hat{\mathbf{x}}, \hat{\phi}) + A\left(\hat{\mathbf{x}}^h, \hat{\phi}\right) \qquad \text{by Equation (17)} \\ &= A\left(\hat{\mathbf{x}}, \hat{\phi}^{\mathcal{I}} - \hat{\phi}\right) - A\left(\hat{\mathbf{x}}^h, \hat{\phi}^{\mathcal{I}} - \hat{\phi}\right) \\ &= L\left(\hat{\phi}^{\mathcal{I}} - \hat{\phi}\right) - A\left(\hat{\mathbf{x}}^h, \hat{\phi}^{\mathcal{I}} - \hat{\phi}\right) \qquad \text{by Equation (8),} \end{aligned} \tag{29}$$

which is a computable estimate of the error provided we know—or have a good enough approximation to—the dual solution $\hat{\phi}$. Alternatively, we can apply the divergence theorem and obtain an error estimator that is very similar to Equation (24).

4.3. Comments on the accuracy of the error estimators

Although we have presented error estimators in Equations (20), (21), (23), (24), (27) and (29), it is clear from the analysis in Sections 4.1 and 4.2 that we may not compute these estimates exactly: we may, however, compute approximations to these estimates as many others have carried out. We have highlighted the approximations that are required as the analysis has been presented. These approximations have also been acknowledged in [21] and are summarised in the succeeding text.

First, in common with all work that uses a dual solution-based *a posteriori* error estimator, we assume that the *exact* dual solution is known. As solving the dual problem is usually as difficult as solving the primal problem, we are unlikely, in general, to be able to write down this exact solution. Instead, in practice, we must be satisfied by a finite element approximation to the dual solution that has been calculated using either a higher order polynomial approximation or has been computed on a finer mesh. Second, for nonlinear problems, the dual solution satisfies a linearised PDE where (assuming that this linearisation exists) the exact linearisation depends on both the true solution and the finite element solution to the primal problem. Clearly, as the true solution is unknown, we cannot perform this linearisation exactly. Again, we must be satisfied with an approximation, and we therefore linearise about the finite element solution. The consequence of this is that there will be errors in the coefficients of the dual problem in Section 4.1.2. The effect of these errors will depend on the sensitivity of the solution to the dual problem to these errors.

DOI: 10.1002/nme

Although the error estimators presented earlier may not be computed exactly, the expectation is that they will be sufficiently accurate that they provide useful information on the precision of the computed functional that may not easily be obtained by other means. For example, we expect that these estimators will correctly identify regions of the computational domain where the mesh should be adapted. As the mesh is adapted in these regions, calculation of the functional will be more accurate, and it is hoped that the estimates will become sharper. The effect of these approximations on the these error estimators is investigated in Section 6 through calculation of effectivity ratios that demonstrate the accuracy of the estimator.

5. THE STRUCTURE OF THE LINEAR SYSTEMS ARISING

The primal finite element problem, Equation (9), results in an algebraic nonlinear system for the unknowns of the finite element approximation to find $\hat{\mathbf{x}}^h \in \left[P_E^k(\Omega)\right]^d \times P^{k-1}(\Omega)$. This nonlinear system of algebraic equations will usually be solved using Newton's method. At each iteration of Newton's method, we calculate the residual vector $\mathbf{R}$ by substituting the current iterate for the solution into Equation (9). A linear system must then be solved that is based on the Jacobian matrix, M_k, which arises from partial differentiation of $\mathbf{R}$ with respect to the unknowns of the finite element approximation. Provided the vector of unknowns is structured in such a way that the unknowns corresponding to the Lagrange multiplier are the last entries in this vector, the Jacobian matrix may be written in the saddle point form

$$M_k = \begin{pmatrix} A & -B^\top \\ B & 0 \end{pmatrix}.$$

The dual solution is usually approximated by computing the finite element solution of the dual problem using the same mesh as for the primal problem but with a polynomial approximation one order higher, that is, we seek a solution in the space $\left[P_E^{k+1}(\Omega)\right]^d \times P^k(\Omega)$ for (different) Dirichlet boundary conditions. The matrix arising from this linear system is $M_{k+1}^\top$, which maintains the saddle point structure. Other linear systems, for example finite element discretisations of the Navier–Stokes equations, also have this structure: for details on suitable preconditioning techniques for solving the linear systems arising, see Elman *et al.* [14].

6. NUMERICAL COMPUTATIONS

We now apply the theory developed in the previous text to three model problems. The first model problem is a manufactured example with a known solution, allowing a validation of the *a posteriori* error estimators. The other examples model a body with part of the boundary fixed and the remainder deforming under the action of gravity. The examples in this section are all in two dimensions, and so we use the notation $\mathbf{X} = (X, Y)^\top$, $\mathbf{x} = (x, y)^\top$ rather than the subscript notation used earlier.

6.1. Model problem 1

Our model problem is governed by Equations (1)–(5). We take Ω to be the unit square $0 < X, Y < 1$. The Dirichlet boundary $\partial\Omega_D$ is the edge $X = 0$, and the remainder of the boundary is the Neumann boundary $\partial\Omega_N$. The strain energy function used, for constants $c_1, c_2 > 0$, is

$$W = c_1 \exp\left(c_2\left(F_{iM}F_{iM} - d\right)\right). \tag{30}$$

This strain energy function may be written in terms of entries of the Green–Lagrange strain tensor discussed in Section 2 as

$$W = c_1 \exp\left(2c_2 \operatorname{trace}(E)\right),$$

and is commonly used to model biological soft tissues [3, 38]. Defining

$$\begin{aligned} \lambda &= 1 + aX, \\ \alpha &= c_2\left(\lambda^2 + \lambda^{-2} + a^2Y^2\lambda^{-4} - 2\right), \end{aligned} \tag{31}$$

DOI: 10.1002/nme

where a is constant, we specify the body force $\mathbf{g}$ as

$$\mathbf{g} = -\frac{2c_1c_2\mathrm{e}^{\alpha}}{\rho}\begin{pmatrix} a + \lambda\frac{\partial\alpha}{\partial X} \\ 2\lambda^{-3}a^2Y - \lambda^{-2}aY\frac{\partial\alpha}{\partial X} + \lambda^{-1}\frac{\partial\alpha}{\partial Y} \end{pmatrix}. \tag{32}$$

We fix the Dirichlet boundary so that

$$\mathbf{x} = \mathbf{X}, \qquad \text{on } X = 0.$$

We apply the following Neumann boundary conditions

$$\mathbf{s} = 2c_1c_2\begin{pmatrix} 0 \\ \lambda - \lambda^{-1}\mathrm{e}^{\alpha} \end{pmatrix}, \qquad Y = 0, \tag{33}$$

$$\mathbf{s} = 2c_1c_2\begin{pmatrix} -a\lambda^{-2} \\ \lambda^{-1}\mathrm{e}^{\alpha} - \lambda \end{pmatrix}, \qquad Y = 1, \tag{34}$$

$$\mathbf{s} = 2c_1c_2\begin{pmatrix} (1+a)\mathrm{e}^{\alpha} - (1+a)^{-1} \\ -aY\,(1+a)^{-2}\,\mathrm{e}^{\alpha} \end{pmatrix}, \qquad X = 1. \tag{35}$$

These body forces and boundary conditions give solution

$$x = X + \frac{1}{2}aX^2, \tag{36}$$

$$y = Y\,(1 + aX)^{-1}, \tag{37}$$

$$p = 2c_1c_2, \tag{38}$$

and the following tensors

$$F = \begin{pmatrix} \lambda & 0 \\ -aY\lambda^{-2} & \lambda^{-1} \end{pmatrix},$$
$$S = 2c_1c_2\begin{pmatrix} \lambda\mathrm{e}^{\alpha} - \lambda^{-1} & -aY\lambda^{-2}\mathrm{e}^{\alpha} \\ -aY\lambda^{-2} & \lambda^{-1}\mathrm{e}^{\alpha} - \lambda \end{pmatrix}.$$

The undeformed body and the solution for $a = 2$ (which will be used in our simulations) is plotted in Figure 1(a). This solution has nonlinear strain tensor with maximum eigenvalue approximately 4.025 at the point $X = Y = 1$. It is clear that linearisation of either the strain tensor or stress tensor is not appropriate in this case. To illustrate the steep gradients in the force acting on the body shown in Figure 1(a), we plot the function $\alpha(X, Y)$, given by Equation (31) in Figure 1(b). Note that the exponential of α appears in the body force given by Equation (32) and all the traction boundary conditions given by Equations (33)–(35). This results in variations of over three orders of magnitude in the body forces acting over the computational domain.

6.1.1. Details of computations. In all the simulations in the succeeding text, we used a regular grid of $2 \times N \times N$ elements—that is, a grid of $N \times N$ squares, each divided into two triangular elements, as shown in Figure 2 for $N = 4$. We used the boundary conditions and body forces described in Section 6.1, with parameters $a = 2$, $c_1 = c_2 = \rho = 1$. In all computations, we sought a solution $\hat{\mathbf{x}}^h \in \left[P_E^2(\Omega)\right]^2 \times P^1(\Omega)$ for the primal finite element problem and a solution $\hat{\phi} \in \left[P_E^3(\Omega)\right]^2 \times P^2(\Omega)$ (or some suitable subspace of this polynomial function space) to approximate the true solution of the dual problem. The interpolant $\hat{\phi}^{\mathcal{I}}$ was calculated by interpolating $\hat{\phi}$ onto the same finite element space as $\hat{\mathbf{x}}^h$. The value of h in the convergence plots is defined by $h = 1/N$.

DOI: 10.1002/nme

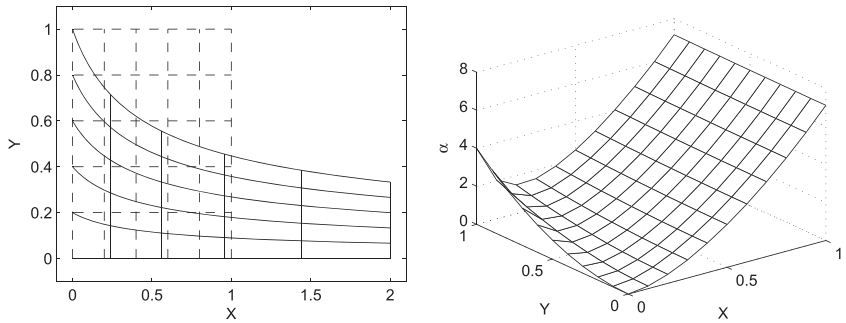

(a) (b)

Figure 1. (a) The deformed body given by Equations (36)–(37) with $a = 2$ (solid lines) and the corresponding lines in the undeformed body (broken lines). (b) The function $\alpha(X, Y)$ given by Equation (31) for $a = 2$ and $c_2 = 1$.

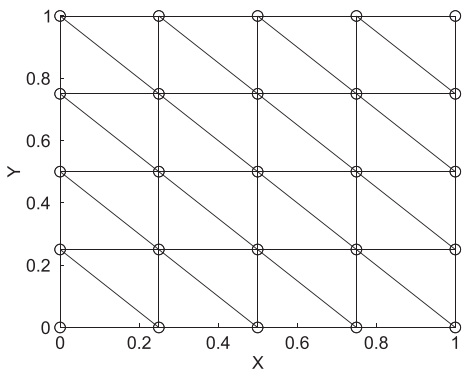

Figure 2. An example mesh used for $N = 4$.

6.1.2. Linear functionals over Ω. We consider three functionals of the form

$$J_i = \int_\Omega \hat{\mathbf{y}}_i \cdot \hat{\mathbf{x}} \, \mathrm{d}V, \qquad i = 1, 2, 3.$$

These functionals are specified by

$$\hat{\mathbf{y}}_1(\mathbf{X}) = (1,\ 1,\ 0)^\top, \tag{39}$$

$$\hat{\mathbf{y}}_2(\mathbf{X}) = (0,\ \delta(X-1)\delta(Y-1),\ 0)^\top, \tag{40}$$

$$\hat{\mathbf{y}}_3(\mathbf{X}) = (0,\ \delta(X-1)\delta(Y),\ 0)^\top, \tag{41}$$

where the function $\delta(p)$ is the Dirac delta function.

The functional J_1 computes the sum of the coordinates of the centre of mass of the deformed body and has true value

$$J_1(\hat{\mathbf{x}}) = \frac{1}{2} + \frac{a}{6} + \frac{\log(1+a)}{2a}. \tag{42}$$

When $a = 2$, this approximately takes the value 1.1080. The functionals J_2 and J_3 correspond to the value of y evaluated at the points $X = 1, Y = 1$ and $X = 1, Y = 0$, respectively, and have true value $1/3$ and 0.

DOI: 10.1002/nme

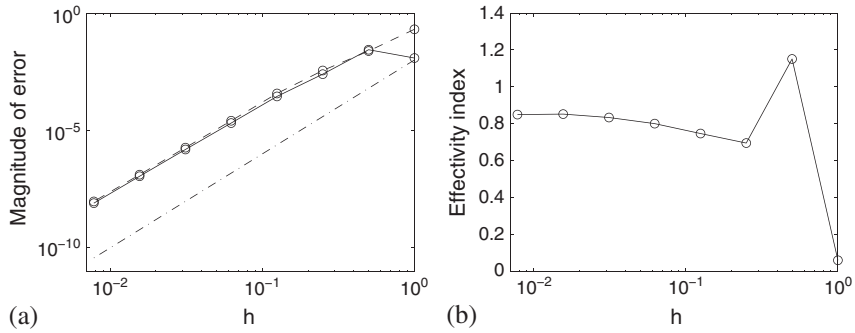

Figure 3. Convergence for the functional J_1. (a) The true magnitude of the error (solid line) and the error estimator for the computations with functional given by Equation (39) (broken line) as a function of h. The dot–dashed line has slope 4. (b) The effectivity index of the error as a function of h.

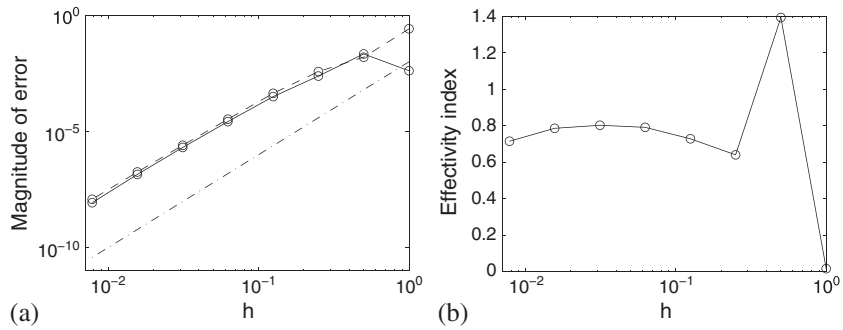

Figure 4. Convergence for the functional J_2. (a) The true magnitude of the error (solid line) and the error estimator for the computations with functional given by Equation (40) (broken line) as a function of h. The dot–dashed line has slope 4. (b) The effectivity index of the error as a function of h.

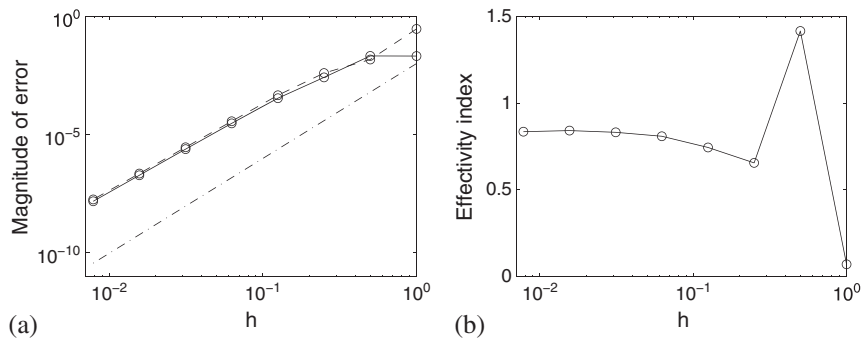

Figure 5. Convergence for the functional J_3. (a) The true magnitude of the error (solid line) and the error estimator for the computations with functional given by Equation (41) (broken line) as a function of h. The dot–dashed line has slope 4. (b) The effectivity index of the error as a function of h.

Convergence plots for J_1, J_2 and J_3 are shown in Figures 3(a), 4(a) and 5(a). For all of these plots, we see that the magnitude of both the error in the computed functional (solid line) and the error estimator (broken line) converges such as h^4 as $h \to 0$ in agreement with the analysis of Pierce and Giles [25] for general nonlinear problems. As would be expected, in all cases, the error estimators given by Equations (20), (21), (23) and (24) give identical values. Effectivity ratios, defined to be the ratio of the magnitude of the true error to the magnitude of the error estimator, for the error estimators are given in Figures 3(b), 4(b) and 5(b). We see from these plots that the error estimators are reasonably sharp for h sufficiently small, although not as close to unity as would be desired. This

DOI: 10.1002/nme

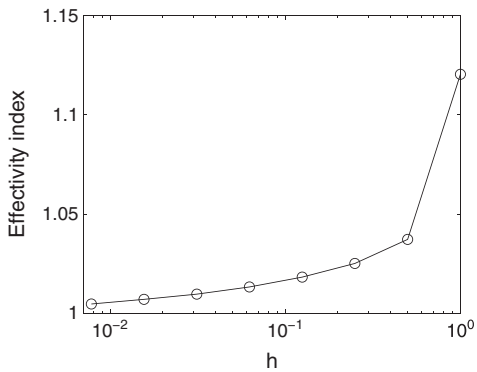

Figure 6. The effectivity index for J_1 when $a = 0.5$.

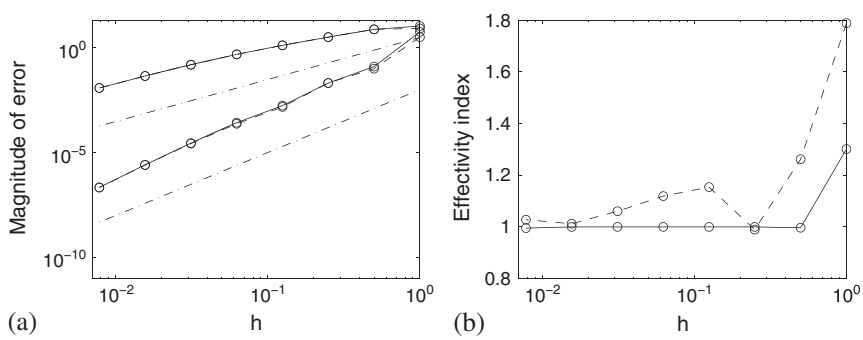

Figure 7. Convergence for the functional J_4. (a) The true magnitude of the error (solid line) and the error estimator (broken line). For the top set of lines, the functional is calculated using Equation (25), and the error estimator is calculated by direct calculation using Equation (27). The dot–dashed line under this top set of lines has slope 2. For the bottom set of lines, the functional is calculated using Equation (28), and the error estimator is calculated by indirect calculation using Equation (29). The dot–dashed line under this top set of lines has slope 3. (b) Effectivity index of the error estimator for the direct calculation (solid line) and the indirect calculation (broken line).

is due to the large variations in body forces and applied forces discussed earlier. To demonstrate this, we plot the effectivity index for calculation of J_1 when $a = 0.5$ (thus giving a smaller deformation) in Figure 6. We see in this figure that, for this smaller value of a, where the magnitude of both the body forces and applied forces varies less rapidly, the effectivity index is much closer to unity.

6.1.3. Functionals over $\partial\Omega_D$. We now consider a functional that is a linear functional of the (non-linear) stress over the Dirichlet boundary. We use a functional corresponding to the moment of the force exerted on the Dirichlet boundary of the deformed body about the point $(0 \quad 0)^\top$. This is achieved by setting $\hat{\mathbf{y}} = (Y \quad 0 \quad 0)^\top$ and then

$$J_4 = \int_{\partial\Omega_D} \mathbf{y} \cdot \mathbf{t} \, \mathrm{d}S,$$

where $\mathbf{t} = S^\top \mathbf{N}$. We again use $c_1 = c_2 = \rho = 1$ in Equations (1)–(30), and $a = 2$. The true value is

$$J_4(\hat{\mathbf{x}}) = \frac{c_1}{a^2}\left(c_2 a^2 + 1 - \mathrm{e}^{c_2 a^2}\right).$$

We first calculate the value of the functional by the direct method of substituting the finite element solution into Equation (25). In Figure 7(a), the top lines compare the magnitude of the true error from Equation (25) (solid line) with the error estimator given by Equation (27) (broken line). The dot–dashed line below these lines has slope 2, and so we may deduce that the computation of the

DOI: 10.1002/nme

functional is second order in h as $h \to 0$. We then evaluate the functional using the indirect method of substituting the finite element solution into Equation (28). The lower solid line in Figure 7(a) is the magnitude of the error that arises from using this approach, and the lower broken line is the magnitude of the error estimator given by Equation (29). The dot–dashed line underneath these lines has slope 3, and so we see that this method gives a faster convergence—third order—as $h \to 0$, as has been observed by other authors [28, 33–36]. Effectivity plots for the error estimators given by the direct evaluation (solid line) and the indirect evaluation (broken line) are given in Figure 7(b). We see that, although the direct method is only second order, the error estimator is very sharp, being very close to unity for all but the largest values of h used.

6.1.4. Adaptive computations. We may use the error estimators given by Equations. (20), (21), (23) and (24) to drive an adaptive mesh strategy. Here, we use the error estimator given by Equation (24). Having solved the primal and dual problems, we write the total error, $\mathcal{E}_{\text{tot}}$, as the sum of the contributions from individual elements

$$\mathcal{E}_{\text{tot}} = \sum_{\kappa} \mathcal{E}_{\kappa},$$

where $\mathcal{E}_{\kappa}$ is the total error from the error estimator associated with element κ. Clearly, any contribution to the error from an integral over element κ is included in $\mathcal{E}_{\kappa}$. Any contribution from the boundary of the domain $\partial\Omega$ is included in the contribution from the element that intersects with the boundary at that point. Contributions across internal boundaries between two elements κ_i and κ_j are divided equally between these two elements. Having calculated the contributions to the error estimator from each element, we then mark elements for refinement, if required. An element κ_i is marked for refinement if

$$\frac{\left|\mathcal{E}_{\kappa_i}\right|}{\sum_{\kappa} |\mathcal{E}_{\kappa}|} > \text{TOL},$$

where TOL is the specified tolerance for the functional of interest. Elements marked for refinement are subdivided into four triangles by placing a node at the midpoint of each edge of the element and joining these new nodes to form four triangles. This may result in hanging nodes in the refined mesh. If an element contains two or more hanging nodes, then this element is refined in the same way as an element marked for refinement. If an element has one hanging node, then this hanging node is joined to the opposite node to subdivide the original element into two elements. This process of removing hanging nodes is repeated until no hanging nodes remain. The primal and dual problems are then resolved on the refined mesh, and further refinement performed, until $\mathcal{E}_{\text{tot}} < \text{TOL}$.

For each of the functionals J_1, J_2, J_3 and J_4 given in Sections 6.1.2 and 6.1.3, we set the tolerance to be the magnitude of the true error calculated in that functional on the finest mesh used earlier, namely a mesh of $2 \times 128 \times 128$ triangular elements with 148 739 DOFs. These tolerances are given in Table I. We begin with a mesh of two triangular elements and adapt the mesh as previously described until the error in the solution is less than the specified tolerance. The DOFs required for each of the functionals are shown in Table I, and the final meshes are shown in Figure 8.

Table I. The number of DOFs in adaptive meshes that were generated when given a tolerance equal to the error on a uniform grid of $2 \times 128 \times 128$ triangular elements, with 148 739 DOFs.

Functional	Tolerance	DOFs	Final error
J_1	9.40×10^{-9}	89 536	5.39×10^{-9}
J_2	1.19×10^{-8}	77 448	3.40×10^{-9}
J_3	1.19×10^{-8}	108 599	1.09×10^{-8}
J_4	2.18×10^{-7}	52 438	5.66×10^{-8}

DOI: 10.1002/nme

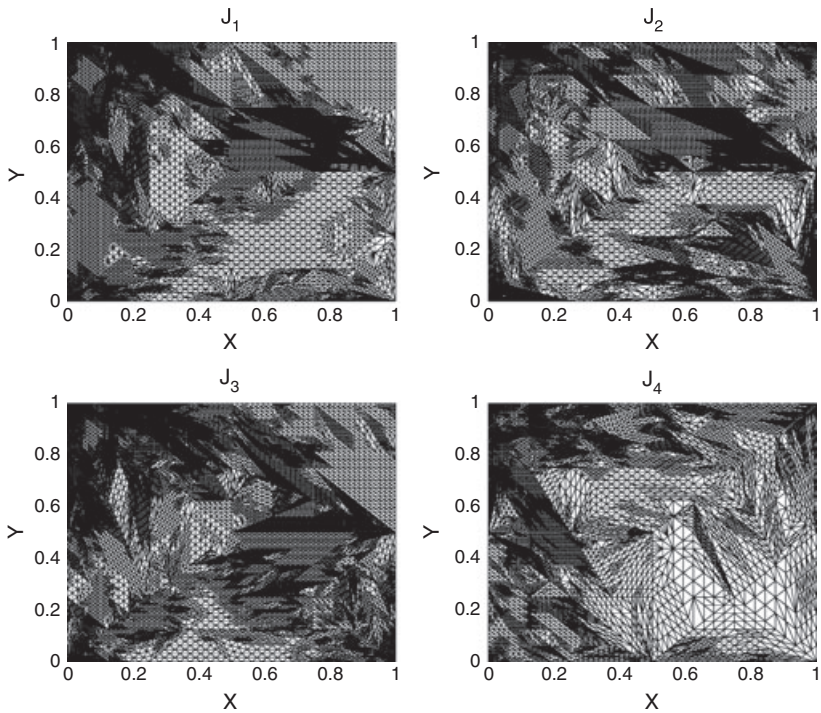

Figure 8. The meshes generated when computing the functionals $J_1, J_2, J_3 and J_4$ to the degrees of accuracy given in Table I.

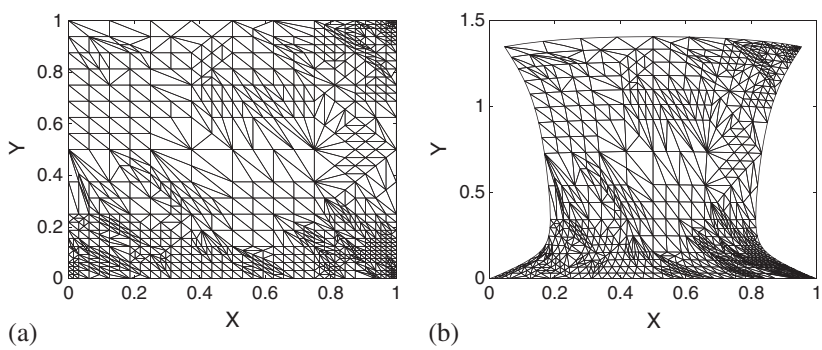

Figure 9. The adapted mesh and the solution for model problem 2.

6.2. *Model problem 2*

For our second model problem, we again take Ω to be the unit square $0 < X, Y, < 1$. In these simulations, we apply a constant body force $\mathbf{g} = (0, 10)^{\top}$. The region on which we prescribe Dirichlet boundary conditions, $\partial\Omega_D$, is the edge $Y = 0$. On this Dirichlet boundary, we specify zero displacement, and so $\mathbf{x} = \mathbf{X}$ for $\mathbf{X} \in \partial\Omega_D$. On the remainder of the boundary, $\partial\Omega_N$, we apply zero stress Neumann boundary conditions. We again use the exponential strain energy function given by Equation (30), with parameters $c_1 = c_2 = \rho = 1$. We use the adaptivity algorithm presented in the previous text to generate an adaptive mesh so that the value of y at the point $X = 1, Y = 1$ is computed to within a tolerance of 10^{-5}. The resulting mesh is shown in Figure 9(a), and the resulting solution with the mesh imposed upon it is shown in Figure 9(b).

We see in Figure 9 that the resulting mesh is heavily adapted in three regions, two regions near to the points where the Dirichlet and Neumann boundaries meet (and where large strains that affect the whole displacement occur) and also near the point of interest.

DOI: 10.1002/nme

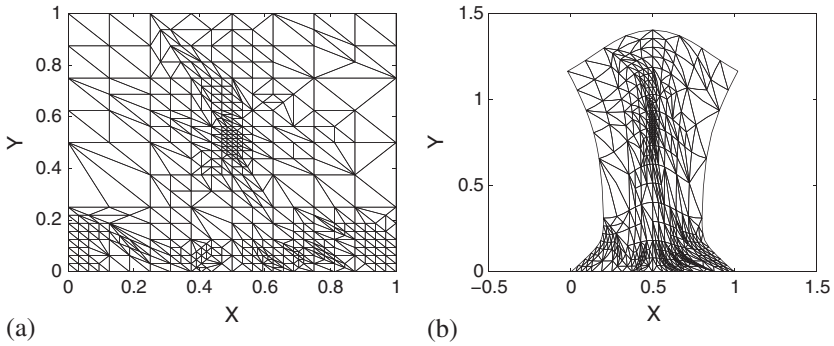

Figure 10. The adapted mesh and the solution for model problem 3.

6.3. *Model problem 3*

Our third model problem is similar to the aforementioned model problem 2, except with two differences. First, the density of tissue is a function of **X** to model a circular region of denser tissue with radius 0.5 inserted into the centre of the square, specifically

$$\rho = \begin{cases} 0.001, & \sqrt{(X-0.5)^2 + (Y-0.5)^2} > 0.25, \\ 5, & \sqrt{(X-0.5)^2 + (Y-0.5)^2} < 0.25. \end{cases}$$

The second difference is that the quantity of interest is the value of y at the point $X = 0.5, Y = 0.5$: this quantity is again computed to within a tolerance of 10^{-5}. The resulting mesh is shown in Figure 10(a), and the resulting solution with the mesh imposed upon it is shown in Figure 10(b). In common with model problem 2, we see refinement in the regions near where the Dirichlet and Neumann boundaries meet and also near the point of interest. Other regions, particularly those occupied by less dense tissue, require far less adaptivity.

7. DISCUSSION

We have presented *a posteriori* error estimators for various functionals of the solution of the equations governing nonlinear, incompressible hyperelasticity. The analysis used to derive these error estimators takes account of nonlinearities both in the calculation of the strain tensor and in the relationship between the entries of the stress tensor and the entries of the strain tensor. Two classes of linear functionals were considered: those that were weighted integrals of the solution over the whole domain and those that were weighted integrals of the stress on a boundary where Dirichlet boundary conditions were prescribed. For the second class of problems, a higher-order method for calculating the functional was presented. The error estimators were then used to drive an adaptive mesh adaptation strategy so that the solution could be computed to within a prescribed tolerance.

These error estimators were tested using a manufactured model problem with a known solution that generated both large deformations and large entries in the (nonlinear) strain tensor. All of the error estimators converged at the expected rate for this problem. Although the error estimators were not as sharp as could be desired for the problem with large deformations, application to a problem with smaller, yet still reasonably large, deformations demonstrated that the effectivity ratio of the estimator (i.e. the ratio of the error estimate to the true error) did approach unity as the mesh was refined. A mesh adaptation strategy based on element-wise contributions to the estimated error was applied to both the manufactured model problem and two further model problems. This strategy produced solutions to within prescribed tolerances in given quantities of interest using significantly fewer DOFs than required when using uniform meshes, indicating that this strategy has practical uses.

DOI: 10.1002/nme

ACKNOWLEDGEMENTS

This research was supported in part by award no. KUK-C1-013-04, made by King Abdullah University of Science and Technology (KAUST). Both authors would also like to acknowledge financial support through the Colorado State University, College of Natural Sciences International Scholars program.

REFERENCES

1. Howell P, Kozyreff G, Ockendon J. *Applied Solid Mechanics*. Cambridge University Press: Cambridge UK, 2009.
2. Nash MP, Hunter PJ. Computational mechanics of the heart. *Journal of Elasticity* 2000; **61**:112–141.
3. Pathmanathan P, Gavaghan DJ, Whiteley JP, Chapman SJ, Brady JM. Predicting tumour location by modelling the deformation of the breast. *IEEE Transactions on Biomedical Engineering* 2008; **55**:2471–2480.
4. Veronda DR, Westmann RA. Mechanical characteristics of skin—finite deformations. *Journal of Biomechanics* 1970; **3**:111–122.
5. Cotin S, Delingette H, Ayache N. Real-time elastic deformations of soft tissues for surgery simulation. *IEEE Transactions on Visualization and Computer Graphics* 1999; **5**:62–73.
6. Chen CY, Byrne HM, King JR. The influence of growth-induced stress from the surrounding medium on the development of multicell spheroids. *Journal of Mathematical Biology* 2001; **43**:191–220.
7. Ball JM. Convexity conditions and existence theorems in nonlinear elasticity. *Archives of Rational Mechanics and Analysis* 1977; **63**:337–403.
8. Oden JT. Recent developments in the theory of finite element approximations of boundary value problems in nonlinear elasticity. *Computer Methods in Applied Mechanics and Engineering* 1979; **17/18**:183–202.
9. Walton JR, Wilber JP. Sufficient conditions for strong ellipticity for a class of anisotropic materials. *International Journal on Nonlinear Mechanics* 2003; **38**:441–455.
10. Babuska I, Suri M. On locking and robustness in the finite element method. *SIAM Journal on Numerical Analysis* 1992; **29**:1261–1293.
11. Babuska I, Suri M. Locking effects in the finite element approximation of elasticity problems. *Numerische Mathematik* 1992; **62**:439–463.
12. Carstensen C, Dolzmann G, Funken SA, Helm DS. Locking-free adaptive mixed finite element methods in linear elasticity. *Computer Methods in Applied Mechanics and Engineering* 2000; **190**:1701–1718.
13. Houston P, Schötzau D, Wihler TP. An hp-adaptive mixed discontinuous Galerkin FEM for nearly incompressible linear elasticity. *Computer Methods in Applied Mechanics and Engineering* 2006; **195**:3224–3246.
14. Elman H, Silvester DJ, Wathen AJ. *Finite Elements and Fast Iterative Solvers*. Oxford University Press: Oxford UK, 2005.
15. Whiteley JP, Gavaghan DJ, Chapman SJ, Brady JM. Nonlinear modelling of breast tissue. *Mathematical Medicine and Biology* 2007; **24**:327–345.
16. Nobile F, Quarteroni A, Ruiz–Baier R. An active strain electromechanical model for cardiac tissue. *International Journal for Numerical Methods in Biomedical Engineering* 2012; **28**:52–71.
17. Rossi S, Ruiz–Baier R, Pavarino LF, Quarteroni A. Orthotropic active strain models for the numerical simulation of cardiac biomechanics. *International Journal for Numerical Methods in Biomedical Engineering* 2012; **28**:761–788.
18. Pathmanathan P, Gavaghan DJ, Whiteley JP. A comparison of numerical methods used for finite element modelling of soft tissue deformation. *Journal of Strain Analysis* 2009; **44**:391–406.
19. Pathmanathan P, Whiteley JP. A numerical method for cardiac mechanoelectric simulations. *Annals of Biomedical Engineering* 2009; **37**:860–873.
20. Eriksson K, Estep D, Hansbo P, Johnson C. Introduction to adaptive methods for differential equations. *Acta Numerica* 1995; **4**:105–158.
21. Giles MB, Süli E. Adjoint methods for PDEs: *a posteriori* error analysis and postprocessing by duality. *Acta Numerica* 2002; **11**:145–236.
22. Rannacher R, Suttmeier FT. *A posteriori* error estimation and mesh adaptation for finite element models in elasto-plasticity. *Computer Methods in Applied Mechanics and Engineering* 1999; **176**:333–361.
23. Ainsworth M, Oden JT. *A posteriori* error estimation in finite element analysis. *Computer Methods in Applied Mechanics and Engineering* 1997; **142**:1–88.
24. Becker R, Rannacher R. An optimal control approach to *a posteriori* error estimation in finite element methods. *Acta Numerica* 2001; **10**:1–102.
25. Pierce NA, Giles MB. Adjoint recovery of superconvergent functionals from PDE approximations. *SIAM Review* 2000; **42**:247–264.
26. Gatica GN, Gatica LF. On the *a priori* and *a posteriori* error analysis of a two-fold saddle-point approach for nonlinear elasticity. *International Journal of Numerical Methods in Engineering* 2006; **68**:861–892.
27. Gatica GN, Gatica LF, Stephan EP. A dual-mixed finite element method for nonlinear incompressible elasticity with mixed boundary conditions. *Computer Methods in Applied Mechanics and Engineering* 2007; **196**:3348–3369.
28. Harriman K, Gavaghan DJ, Houston P, Süli E. Adaptive finite element simulation of currents at microelectrodes to a guaranteed accuracy. *Electrochemistry Communications* 2000; **2**:157–162.
29. Larsson F, Hansbo P, Runesson K. Strategies for computing *a posteriori* error measures in nonlinear elasticity. *International Journal for Numerical Methods in Engineering* 2002; **55**:879–894.

DOI: 10.1002/nme

30. Barrientos MA, Gatica GN, Stephan EP. A mixed finite element method for nonlinear elasticity: two-fold saddle approach and *a-posteriori* error estimate. *Numerische Mathematik* 2002; **91**:197–222.
31. Larsson F, Dìez P, Huerta A. A flux-free *a posteriori* error estimator for the incompressible Stokes problem using a mixed FE formulation. *Computer Methods in Applied Mechanics and Engineering* 2010; **199**:2383–2402.
32. Rüter M, Stein E. Analysis, finite element computation and error estimation in transversely isotropic nearly incompressible finite elasticity. *Computer Methods in Applied Mechanics and Engineering* 2000; **190**:519–541.
33. Babuska I, Miller A. The post-processing approach in the finite element method—Part 1: calculation of displacements, stresses and other higher derivatives of the displacements. *International Journal for Numerical Methods in Engineering* 1984; **20**:1085–1109.
34. Babuska I, Miller A. The post-processing approach in the finite element method—Part 2: the calculation of stress intensity factors. *International Journal for Numerical Methods in Engineering* 1984; **20**:1111–1129.
35. Babuska I, Miller A. The post-processing approach in the finite element method—Part 3: *a posteriori* error estimates and adaptive mesh selection. *International Journal for Numerical Methods in Engineering* 1984; **20**:2311–2324.
36. Harriman K, Gavaghan DJ, Houston P, Süli E. Adaptive finite element simulation of currents at microelectrodes to a guaranteed accuracy. *Application to a simple model problem. Electrochemical Communications* 2000; **2**:150–156.
37. Ortner C, Süli E. Discontinuous Galerkin finite element approximation of nonlinear second order elliptic and hyperbolic systems. *SIAM Journal on Numerical Analysis* 2007; **45**:1370–1397.
38. Costa KD, Holmes JW, McCulloch AD. Modelling cardiac mechanical properties in three dimensions. *Philosophical Transactions of the Royal Society of London A* 2001; **359**:1233–1250.

DOI: 10.1002/nme